Molecular Crystals and Liquid Crystals
Publication details, including instructions for authors and subscription information:
http://www.tandfonline.com/loi/gmcl20

Electron Transport Mechanism through a Cathode Buffer in Organic Solar Cells

Tatsuya Oida [a] & Kenji Harafuji [a]

[a] Department of Electrical and Electronic Engineering, Ritsumeikan University, 1-1-1 Noji-Higashi, Kusatsu, Shiga, 525-8577, Japan

Version of record first published: 17 Sep 2012.

To cite this article: Tatsuya Oida & Kenji Harafuji (2012): Electron Transport Mechanism through a Cathode Buffer in Organic Solar Cells, Molecular Crystals and Liquid Crystals, 567:1, 44-49

To link to this article: http://dx.doi.org/10.1080/15421406.2012.702379

Mol. Cryst. Liq. Cryst., Vol. 567: pp. 44–49, 2012

ISSN: 1542-1406 print/1563-5287 online
DOI: 10.1080/15421406.2012.702379

Taylor & Francis
Taylor & Francis Group

Electron Transport Mechanism through a Cathode Buffer in Organic Solar Cells

TATSUYA OIDA AND KENJI HARAFUJI*

Department of Electrical and Electronic Engineering, Ritsumeikan University, 1-1-1 Noji-Higashi, Kusatsu, Shiga 525–8577, Japan

A new electron transport mechanism through cathode buffer in organic solar cells is proposed with the inverted structure of indium-tin oxide (cathode)/very thin Ag layer (cathode)/bathocuproine (BCP, buffer)/fullerene/copper phthalocyanine/pentacene/Ag (anode). Electron transport across the BCP occurs not through defect states, but over the LUMO (lowest unoccupied molecular orbital). The electron conductivity is sensitive to the cathode work function (*WF*c). As* WF*c is lower, the energy difference between the BCP LUMO and the cathode Fermi level is smaller. This introduces low electronic potential barrier. The low* WF*c is important to achieve low series resistance.*

Keywords organic solar cells; buffer layer; bathocuproine; electron transport; work function

Organic solar cells (OSCs) have received attention as a renewable energy resource because of its low cost and ease of fabrication. Since Tang presented a concept of donor-acceptor heterojunction in 1986 [1], various ideas for the improvement of OSCs have been proposed. One of them is an "exciton blocking layer (EBL)". In 2000, Peumans presented bathocuproine (BCP) buffer layer inserted between an acceptor layer and a metal cathode as EBL [2]. The EBL protects fullerene (C_{60}, acceptor) from the cathode metal diffusion, and prevents exciton from quenching at the C_{60}/cathode interface. Since then, the cathode buffer layer became an indispensable part for small molecular OSCs. In the last decade, the buffer layer has been extensively investigated, and the other role of BCP as a buffer layer has been presented in the following. The first is an establishment of an ohmic contact between the acceptor layer and the cathode [3]. The second is a prevention of reversing polarity of built-in-field [4]. The third is an enhancement of built-in-field [5]. The fourth is the role as an optical spacer [6].

The electron transport mechanism through BCP is, however, not necessarily well understood. It has been widely accepted that electrons transport across the BCP layer through defect states below the LUMO induced during the deposition process of cathode [2]. In this paper, a new transport mechanism is proposed by using inverted OSCs from the standpoint of the cathode work function (WF_C).

Figure 1 shows schematics of four kinds of OSCs. In Devices A and B, indium-tin oxide (ITO) plays a role of an cathode. Hereafter, OSCs of this type are called "inverted OSCs". In the inverted OSCs, BCP is evaporated after the cathode metal deposition. Therefore, there is few defect states in the BCP layer. In inverted OSCs, a pentacene thin layer plays

*Address correspondence to Kenji Harafuji. E-mail: harafuji@se.ritsumei.ac.jp

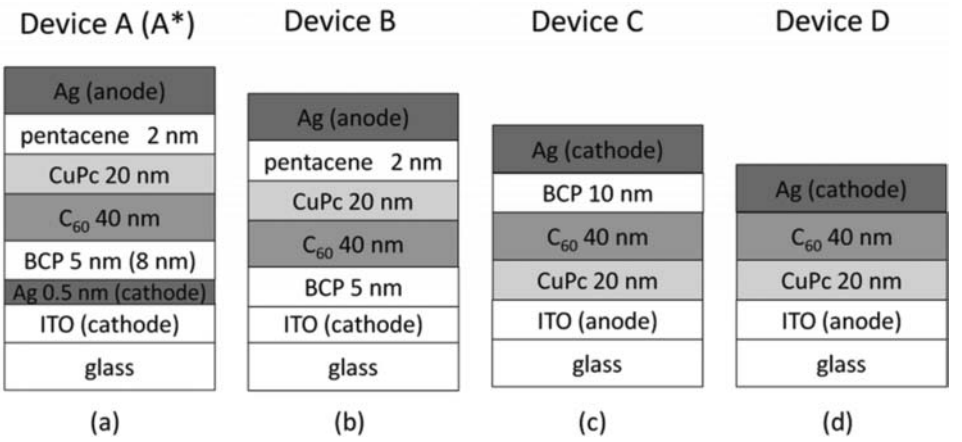

Figure 1. Schematics of four kinds of organic solar cells. (a) Inverted structure with Ag thin layer. (b) Inverted structure without Ag thin layer. (c) Normal structure with BCP buffer layer. (d) Normal structure without BCP buffer layer.

a role of an anode buffer layer to establish the inverted structure [7]. The only difference between Devices A and B is the existence of very thin Ag layer between ITO and BCP. In Devices C and D, ITO plays a role of the anode. Hereafter, OSCs of this type are called "normal OSCs". The only difference between Devices C and D is the existence of BCP buffer layer between C_{60} and Ag. Organic materials are evaporated on the ITO substrate at a rate of 0.5 Å/s, under a pressure of less than 1.0×10^{-3} Pa. The deposition rate is monitored by an oscillation quartz microbalance. All organic materials are used as purchased. The Ag top electrode is thermally evaporated through a stainless mask with 6 mm^2 active area of 2.4×2.5 mm^2. The photovoltaic current density-voltage (*J-V*) measurements are carried out using an electrometer (ADC 6241A) and an electric automatic shutter (Agilent 34970A/34903A). Xenon lamp illumination at intensity of 100 mW/cm^2 is performed and an air mass 1.5 global (AM1.5G) spectrum is obtained using a solar simulator. The intensity of the simulator output is calibrated using crystalline silicon solar cells with a 320–1100 nm broadband. The investigated devices are kept in air at room temperature during the entire measurement procedure without any encapsulation.

Figure 2 shows the typical *J-V* characteristics of Devices A-D under illumination. The device parameters are summarized in Table 1, where J_{sc} is the short-circuit current density, V_{oc} is the open-circuit voltage, *FF* is the fill factor, *n* is the ideality factor, R_s is the series resistance, R_{sh} is the shunt resistance, η_p is the power conversion efficiency. Here, R_s, R_{sh},

Table 1. Device parameters

	J_{SC} (mA/cm^2)	V_{OC} (V)	*FF* (%)	*n*	R_s (Ω cm^2)	R_{sh} (Ω cm^2)	η_p (%)
Device A	2.36	0.38	51.8	2.1	4.8	7.2×10^4	0.46
Device B	1.97	0.34	43.0	1.9	47.3	2.1×10^4	0.28
Device C	3.46	0.45	56.7	2.0	9.6	4.5×10^5	0.88
Device D	3.03	0.39	44.3	2.6	53.3	5.0×10^4	0.53
Device A*	2.20	0.40	52.8	2.2	4.1	2.2×10^4	0.47

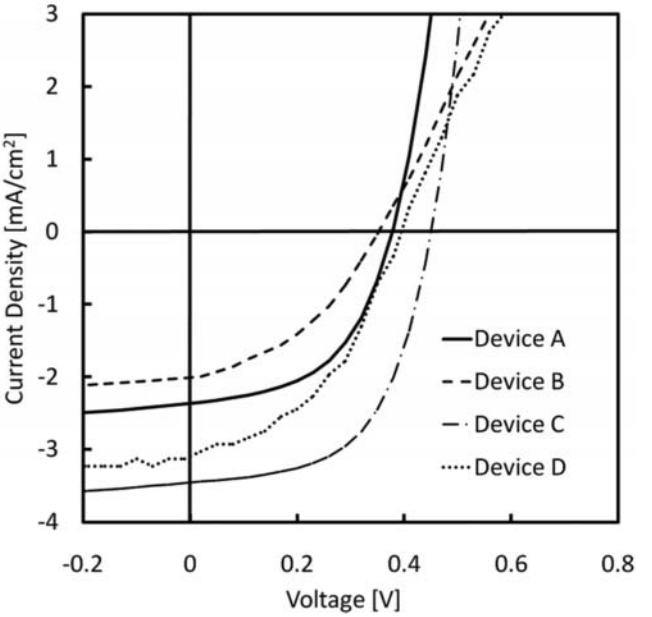

Figure 2. Current-voltage characterictics of four devices.

and n are obtained by fitting an equation of an equivalent circuit model to the dark J-V characteristics. The equation is described by

$$\mathrm{J} = \frac{R_{\mathrm{sh}}}{R_{\mathrm{s}} + R_{\mathrm{sh}}} \left\{ J\mathrm{s}\left[\exp\left\{ \frac{q(V - JR_{\mathrm{s}})}{nkT} \right\} - 1 \right] + \frac{V}{R_{\mathrm{sh}}} \right\}, \tag{1}$$

where k is the Boltzmann constant, T is the temperature, J_{s} is the reverse dark saturation current density, and V is the bias voltage. The ideality factor of all devices is approximately 2.0, and is not much affected by the difference of the device structure. The shunt resistance of all devices is high enough not to affect the other device parameters. Therefore, the discussion will be made by comparing J_{sc}, V_{oc}, FF, R_{s} in each device.

It is seen in Table 1 that Device A demonstrates a higher performance than Device B. Especially, R_{s} in Device A is as small as that in Device C (the normal device). The structural difference between Devices A and B is the existence of the Ag thin layer. So, the improvement in Device A is attributed to the effect of the Ag thin layer. As is described, electrons pass through defect states below the BCP LUMO in the conventional model. In both of Devices A and B, however, cathode metal hardly diffuses into BCP layer, since BCP is deposited after the cathode deposition. Furthermore, a melting point of Ag (= 961.9°C) is higher than a boiling point of BCP (= 531.9°C). Therefore, the low R_{s} of Device A comparable to that of Device C cannot be explained by the conventional model.

A new hypothesis is proposed that photo-induced electrons pass over the LUMO (lowest unoccupied molecular orbital) of BCP into the cathode, and that the electron transport efficiency is sensitive to the cathode material. The Ag cathode is more suitable for low R_{s} than the ITO cathode. It is seen in Table 1 that the performance of Device C is much better than that of Device D, where the cathode for the two devices is Ag. The only difference between them is the existence of the BCP buffer. Accordingly, the high electron

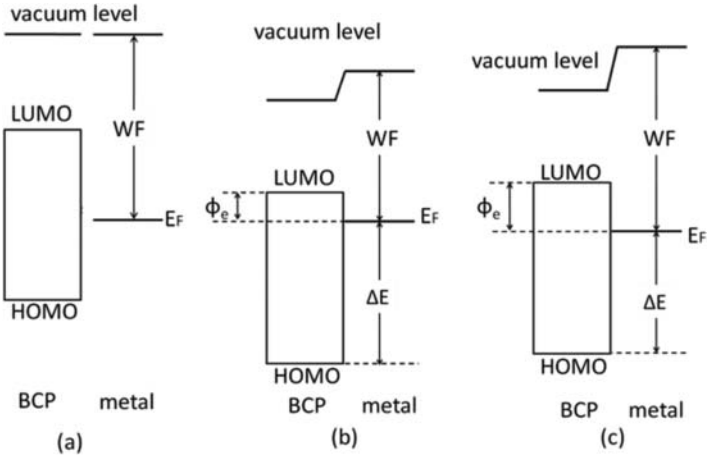

Figure 3. Energy level diagram between metal and C_{60}. (a) Before the contact. (b) After the contact with the metal of low work function *WF*. (c) After the contact with the metal of high work function *WF*.

conductivity is achieved with the combination of the Ag cathode metal and BCP buffer layer. Ag cathode has some kinds of effect on BCP layer for low R_s.

The effect of the Ag thin layer on the electron transport across the BCP is discussed. Toyoshima *et al.* reported the experiment on the BCP/metal interface by ultraviolet photoemission spectroscopy [8]. Figure 3 shows the energy level diagram, where E_F denotes the metal Fermi level. They show that the shift of the highest occupied molecular orbital (HOMO) level, ΔE, to a lower electronic energy increases, as the metal work function (*WF)* decreases. In other words, electronic potential barrier height (φ_e) decreases, as the *WF* of the metal is smaller. Figure 4 shows the electron transport mechanism. Figure 4(a)

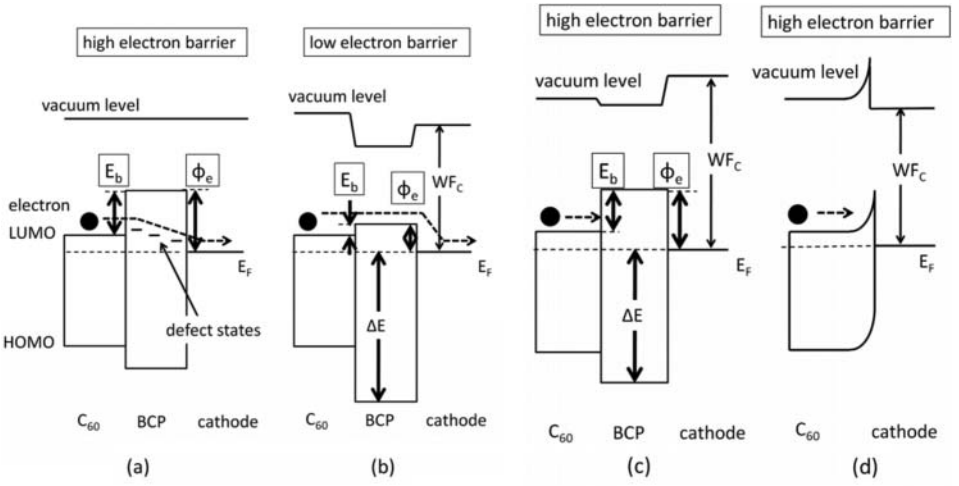

Figure 4. Electron transport mechanism. (a) Conventional model. (b) Proposed model for low WF_C. (c) Proposed model for high WF_C. (d) Schottky barrier model at C_{60}/cathode.

is the conventional model. Figures 4(b) and 4(c) are the proposed mechanism for Devices A,C with Ag cathode (low cathode work function WF_C) and Device B with ITO cathode (high WF_C), respectively. In Fig. 4(b) for Devices A and C, the shift ΔE of BCP HOMO level to the lower electronic energy relative to E_F is large, and the potential barrier height E_b for electron transport is low. As a result, R_s decreases, which leads to higher J_{sc} and FF. In Fig. 4(c) for Device B, the shift of BCP HOMO, ΔE, is small, and the potential barrier height E_b is high. As a result, R_s is large, which leads to smaller J_{sc} and FF. The WF of the thin Ag layer (the cathode of Device A) is 4.3 eV [9], and that of ITO (the cathode of Device B) is 4.7 eV [10]. Therefore, it is understood that the smaller WF_C brings about the lower Rs by comparing Device A with Device B in Table I. Figure 4(d) is the energy level diagram of Device D. Device D is the normal device without BCP buffer layer. At the interface between C_{60} and metal, the Schottky barrier is formed. High R_s of Device D is attributed to the high potential barrier. In Fig. 4(b), the LUMO of BCP plays a role of a bridge between the LUMO of C_{60} and the Fermi level of Ag, and this achieves the ohmic contact.

In order to verify this hypothesis, Device A* is fabricated. The structure of Device A* is the same as that of Device A except for the thickness of BCP buffer layer. The thickness of the BCP layer in Device A* is 3 nm thicker than that in Device A. The performance of Device A* is shown in Table I. The series resistance of Device A* is slightly smaller than that of Device A though the BCP thickness is increased. The decrease of R_s cannot be explained by the conventional electron transport mechanism of Fig. 4(a). That is, photo-induced electrons pass over the LUMO of BCP into the cathode. The decrease of R_s is attributed to a better coverage of BCP over the Ag cathode surface. This brings about a better ohmic contact at BCP/Ag interface.

In summary, electron transport mechanism through a BCP cathode buffer in OSCs is investigated by using inverted solar cells with a structure of ITO (cathode)/very thin Ag layer/BCP/C_{60}/CuPc/pentacene/Ag (anode). It is found that the series resistance R_s of OSC with the thin Ag layer is much lower than that of OSC without the thin Ag layer. The value R_s is comparable to that of the normal OSC with a structure of ITO (anode)/CuPc/C_{60}/BCP/Ag (cathode). The thin Ag layer greatly improves the electron transport efficiency through the BCP layer. That is, when the cathode material is changed from the high work function material (ITO) to the low work function material (Ag), the electron conductivity is increased. The electron conductivity is sensitive to the cathode work function WFc. As WFc is lower, the energy difference between the BCP LUMO and the cathode Fermi level is smaller. That is, the potential barrier height for electron transport through BCP is lower. This indicates that electron transport across the BCP occurs not through defect states, but over the LUMO of BCP. The low WFc is important to achieve low series resistance.

References

[1] Tang, C. W. (1986). *Appl. Phys. Lett.*, *48*, 183.
[2] Peumans, P., Bulović, V., & Forrest, S. R. (2000). *Appl. Phys. Lett.*, *76*, 2650.
[3] Vogel, M., Doka, S., Breyer, C., Lux-Steiner, M. C., & Fostiropoulos, K. (2006). *Appl. Phys. Lett.*, *89*, 163501.
[4] Song, Q. L., Li, C. M., Wang, M. L., Sun, X. Y., & Hou, X. Y. (2007). *Appl. Phys. Lett.*, *90*, 071109.
[5] Gommans, H., Verreet, B., Rand, B. P., Muller, R., Poortmans, J., Heremans, P., & Genoe, J. (2008). *Adv. Funct. Mater.*, *18*, 3638.
[6] Huang, J., Yu, J., Lin, H., & Jiang, Y. (2009). *J. Appl. Phys.*, *105*, 073105.

[7] Oida, T., Naito, T., Miyagawa, Y., Sasaki, M., & Harafuji, K. (2011). *Jpn. J. Appl. Phys.*, *50*, 081601.
[8] Toyoshima, S., Kuwabara, K., Sakurai, T., Taima, T., Saito, K., Kato, H., & Akimoto, K. (2007). *Jpn. J. Appl. Phys.*, *46*, 2692.
[9] Michaelson, H. B. (1977). *J. Appl. Phys.*, *48*, 4729.
[10] Tang, J. X., Zhou, Y. C., Liu, Z. T., Lee, C. S., & Lee, S. T. (2008). *Appl. Phys. Lett.*, *93*, 043512.